Informative Change Detection by Unmixing for Hyperspectral Images

Alp Erturk, *Member, IEEE*, and Antonio Plaza, *Fellow, IEEE*

***Abstract*—Applying spectral unmixing on a series of multitemporal hyperspectral images for change detection has the potential to reveal important subpixel-level information, such as the abundance variation of each underlying material in a given location or the change in the distribution of materials throughout the scene, with time or resulting from significant events such as a natural disaster. However, change detection by spectral unmixing for hyperspectral images has not been extensively studied up to now, and most studies have been limited to specific cases and data sets. This is caused by the scarcity of real multitemporal hyperspectral data and the inherent difficulties in applying unmixing to multitemporal hyperspectral data in a coherent way. In this letter, we investigate change detection for hyperspectral images by spectral unmixing and systematically present the advantages that can be gained by using such an approach, supported by experimental studies conducted on carefully prepared synthetic data sets and also with real data sets.**

***Index Terms*—Change detection, hyperspectral imaging, spectral unmixing.**

I. Introduction

HYPERSPECTRAL imaging provides an increased capability for many image processing tasks such as classification, detection, and identification, by utilizing the wealth of spectral information contained in the data [1]. Change detection, the process of detecting variations on a scene through the processing of multitemporal images, is used for many applications ranging from environmental monitoring and city planning to detection of pollution, crop stress, and military targets [2].

Global linear predictors are benchmark approaches in hyperspectral change detection. Chronochrome (CC), proposed in [3], is a linear prediction method and relies on finding a linear transformation between two data sets based on joint second-order statistics. Covariance equalization (CE), a similar method based on whitening and proposed in [4], aims to reduce sensitivity to misregistration by not using the cross-covariance matrix. An optional anomaly detection step can be used after either method to detect anomalous changes. Subspace-based change detection (SCD), proposed in [5], aims to detect the changes in one hyperspectral image by using the background subspace of the corresponding pixel in the other image. Elliptically contoured distribution based change detection is proposed in [6] to address the fact that real data are generally not Gaussian. Iteratively reweighted multivariate alteration detection utilized in [7] relies on canonical variants to detect the changes.

Hyperspectral change detection by spectral unmixing, in contrast to other change detection approaches, has the potential to actually provide easily interpretable information on the nature of the change, instead of providing only the locations that exhibit changes in the scene. Spectral unmixing is the process of decomposing pixels into a set of abundances of pure material spectral signatures, which are called *endmembers* [8]. Change detection by unmixing offers the important promise of providing the nature of the change, whether it is a change in the abundances of pure materials in the pixel or the addition/subtraction of an endmember to/from the scene. These variations relate to real-life situations such as a new crop cultivated in a given farmland area (i.e., change of the endmember with the prominent abundance in a given location), natural disasters such as flooding (i.e., change in the abundance of a given endmember throughout the scene), crop stress (i.e., a change in the endmember signature or a new endmember), military targets (i.e., new, possibly anomalous, endmembers in the scene), and so on.

Hyperspectral change detection by unmixing is still in an early stage in the literature, with most studies being limited to case studies with a certain limited problem and a corresponding data set. For instance, [9] presents a general framework for hyperspectral change detection using unsupervised linear unmixing. In [10], subpixel change detection is addressed for a case study using abundance and slope features. In [11], multitemporal unmixing of medium spatial resolution data is discussed with applications in land-cover mapping. The real advantage of change detection by unmixing, i.e., the possibility to obtain more information than the usual one achieved by other change detection techniques, is generally only briefly touched upon, if at all. In this letter, change detection by unmixing is examined in detail, and the information and the advantages that such an approach provides are showcased through systematic experiments on synthetic data sets, in addition to real data.

The remainder of this letter is organized as follows. Section II describes the proposed methodology for change detection by unmixing. Experimental results are provided in Sections III and IV for synthetic and real data sets, respectively. This letter is concluded in Section V, which also includes hints at plausible future research lines.

II. Methodology

Our strategy for hyperspectral change detection by unmixing involves detecting the dimensionality of the data, extracting the pure spectral signatures (endmembers) of the materials in the

Manuscript received November 16, 2014; revised December 15, 2014; accepted January 7, 2015. This work was supported by the Scientific and Technical Research Council of Turkey (TÜBİTAK).

The authors are with the Hyperspectral Computing Laboratory, Department of Technology of Computers and Communications, University of Extremadura, 10003 Cáceres, Spain (e-mail: alp.erturk@kocaeli.edu.tr; aplaza@unex.es).

Color versions of one or more of the figures in this paper are available online at http://ieeexplore.ieee.org.

Digital Object Identifier 10.1109/LGRS.2015.2390973

scene, calculating the abundance maps of the corresponding materials, and then detecting the change in abundance maps through time.

Whereas sparse unmixing with a spectral library would have the advantage of circumventing the need for detecting the number of endmembers and extracting these endmembers [12], constructing the spectral library generally involves significant efforts. For simplicity, in this work, the endmembers are directly extracted from the hyperspectral data; hence, a spectral library with a sparse unmixing approach is not utilized.

Prior to endmember extraction, the number of endmembers, i.e., the actual dimensionality of the data, should be determined. In this letter, hyperspectral signal identification by minimum error (HySime) [13] is utilized for this purpose and applied on the whole multitemporal hyperspectral series, i.e., on all of the hyperspectral data sets acquired from the same scene at different times, in conjunction, instead of on each temporal data set separately. HySime is applied to the whole multitemporal series because endmembers will be extracted from the whole multitemporal data, the reason of which will be explained shortly. It also ensures that the result is more robust.

After the number of endmembers is estimated, endmember extraction is applied to the full multitemporal hyperspectral data set. This results in a common endmember pool and ensures that multiple pixels are not selected for the same endmember in different data sets. Note that, if an endmember is present in one temporal data set and absent in another temporal data set of the same series, it will still be extracted by this approach. Whereas applying HySime and endmember extraction on the whole multitemporal data set gives more robust and stable results, it also results in the simplification that the variability of the spectral signatures of endmembers themselves through time is disregarded. Future studies will address this issue.

There are various endmember extraction algorithms (EEAs) in the literature. Some, like N-FINDR [14] and vertex component analysis (VCA) [15], operate with the assumption that pure materials are available in the scene, while others such as minimum volume simplex analysis [16] and simplex identification via split augmented Lagrangian (SISAL) [17] operate without this assumption but may, in turn, lead to virtual endmembers. In this letter, one method from each category, N-FINDR and SISAL are utilized as the EEAs. However, our proof of concept works with any EEA.

After the endmembers are extracted from the multitemporal data series, fully constrained least squares (FCLS) [18] is used to obtain the abundances in each pixel for each endmember, in each temporal data set. In other words, the endmember set is common, whereas the abundances are determined for each temporal data set separately.

In a last step, the change in each abundance map for each endmember is calculated by a simple difference operation between the corresponding abundance maps of different temporal data sets, and the total change map can be obtained by the summation of the change maps for each endmember.

III. Experiments on Synthetic Data

A. Synthetic Data Set 1

The first synthetic multitemporal data set is simulated from the well-known ROSIS Pavia University data [19]. The temporal data sets belong to the area around the metal building in the scene and are of size $120 \times 70 \times 103$ pixels. The spatial resolution of the data is 1.3 m, and the spectral resolution is 4 nm. A synthetic change between the two temporal data samples is simulated so that the vegetation regions between the parts of the building are modified to dirt in the second temporal data set. This modification is done in terms of abundance, i.e., at subpixel level, and gradually so that diagonally the upper parts of the image have more change than the lower parts. The RGB images of the temporal data sets are provided in Fig. 1.

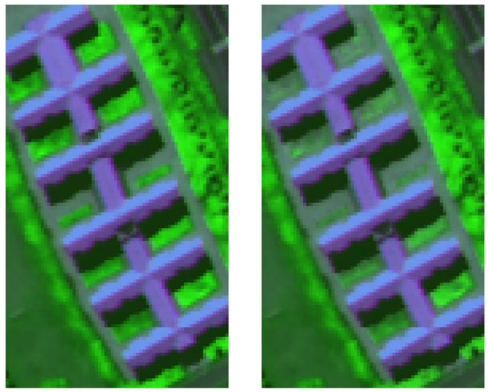

Fig. 1. RGB images for the first synthetic data set.

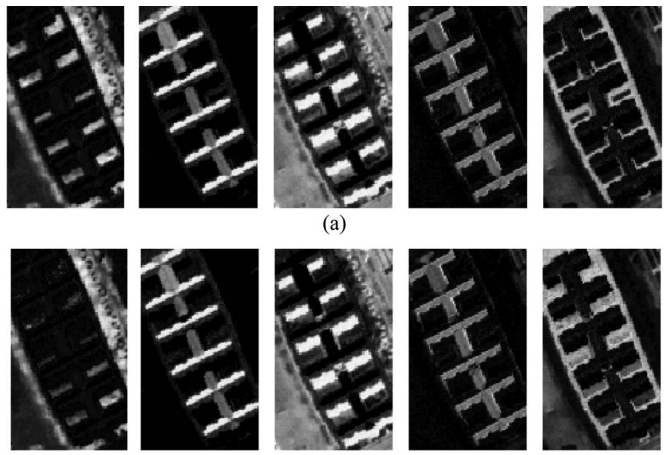

Fig. 2. Abundance maps. (a) For the first temporal data set. (b) For the second temporal data set.

Additive Gaussian white noise with 30-dB signal-to-noise ratio (SNR) is added to each temporal data set. HySime, when applied to the whole multitemporal data set, estimates five endmembers. The endmembers are extracted by N-FINDR from the whole multitemporal data series, and the abundance maps are estimated for each temporal data set. The abundance maps obtained by FCLS are presented in Fig. 2.

It can be observed from Fig. 2 that the significant change is from the first endmember to the fifth endmember, which correspond to vegetation and dirt, respectively. In other words, by using the change detection by unmixing, we can also observe extra information indicating that some pixels with high vegetation abundance have changed to be mostly dirt in the second temporal data set instead of just detecting that there is change in some pixels. It is important that other change detection approaches cannot provide this extra information.

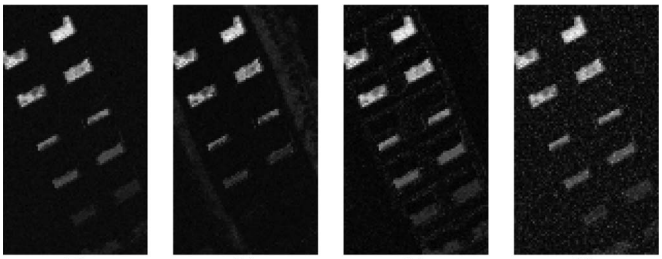

Fig. 3. Change maps for the first synthetic data set. (a) EUC. (b) CC. (c) Unmixing (N-FINDR as EEA). (d) Unmixing (SISAL as EEA).

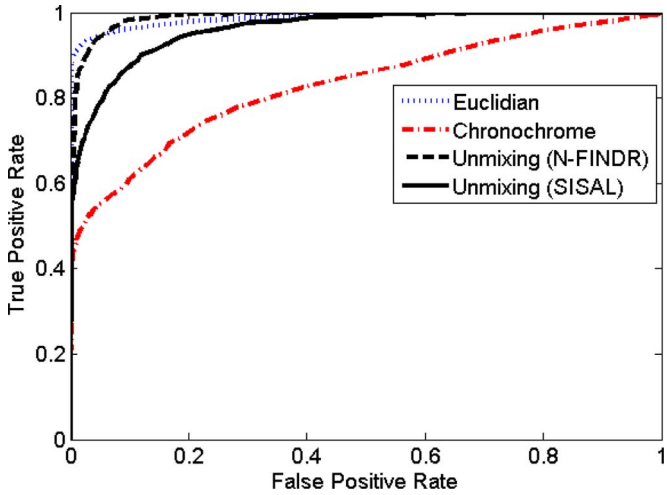

Fig. 4. ROC curves for the first synthetic data set.

Fig. 3 gives a comparison between the change maps obtained by Euclidian distance (EUC), CC, and final change map obtained using the change detection by unmixing approach, with N-FINDR or SISAL as the EEA. In this letter, CC is applied in a global manner, i.e., finding a global transformation matrix instead of local transformation matrices, for computational reasons. The spectral angular distance and CE were also investigated as methods for our experimental results but discarded due to the significantly worse results that they provided in each case. It can be observed from Fig. 3 that the methods perform comparably. However, neither EUC nor CC provides the extra information reported in Fig. 2.

In Fig. 4, receiver-operating-characteristic (ROC) curves are presented for the utilized methods, based on a manually prepared ground truth. Euclidian distance and the proposed change detection by unmixing approaches perform better than CC, and using N-FINDR as the EEA performs better than using SISAL as the EEA, as expected also from Fig. 3.

B. Synthetic Data Set 2

The second synthetic multitemporal data set is also formed from the ROSIS Pavia University data. The data comprise a crossroads in the scene and are of size 75 $\times$ 70 $\times$ 103 pixels. The synthetic change between the two temporal data sets is that the vehicle in the scene is carefully removed in the second data set and the pixels in the corresponding location are modified to pixel information belonging to the road in the background. The pixels that are directly around the vehicle are also modified, at subpixel level, to remove the shadow effects. The RGB images are provided in Fig. 5.

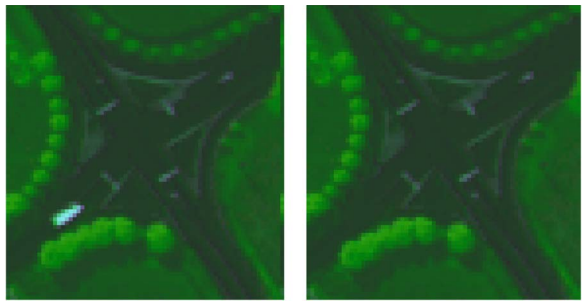

Fig. 5. RGB images for the second synthetic data set.

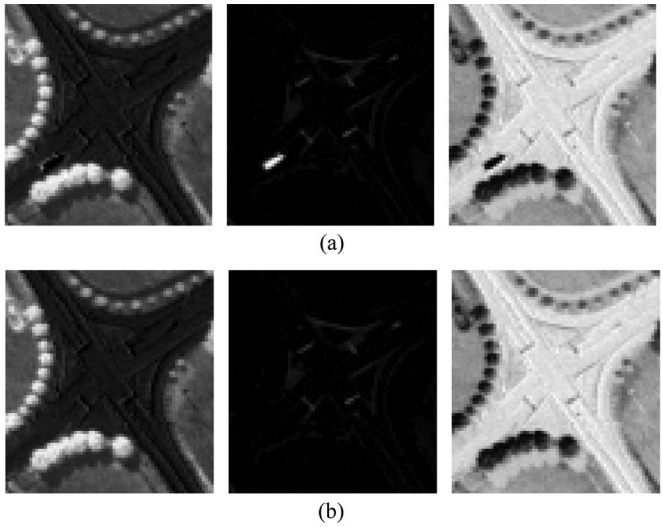

Fig. 6. Abundance maps. (a) For the first temporal data set. (b) For the second temporal data set.

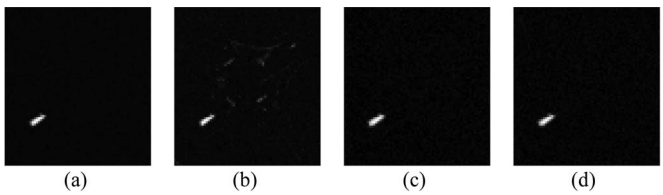

Fig. 7. Change maps for the second synthetic data set. (a) Euclidian distance. (b) CC. (c) Unmixing (N-FINDR as EEA). (d) Unmixing (SISAL as EEA).

Additive Gaussian white noise is added to each data set in 30-dB SNR. HySime estimates the dimensionality as three when applied to the whole multitemporal data set. The abundance maps for each temporal data set, obtained by FCLS based on the endmembers extracted from the multitemporal data by N-FINDR, are provided in Fig. 6. The first endmember is vegetation, the second endmember belongs to the vehicle, and the third endmember can be observed to be a combination of road and shadow. Fig. 6 reveals that the second endmember is not present in the second temporal data set, and the corresponding pixels are now a combination of road and shadow.

The final change maps obtained by EUC, CC, and the proposed change detection by unmixing approach, with N-FINDR or SISAL as the EEA, are provided in Fig. 7. It can be observed that the results are comparable. In Fig. 8, ROC curves are

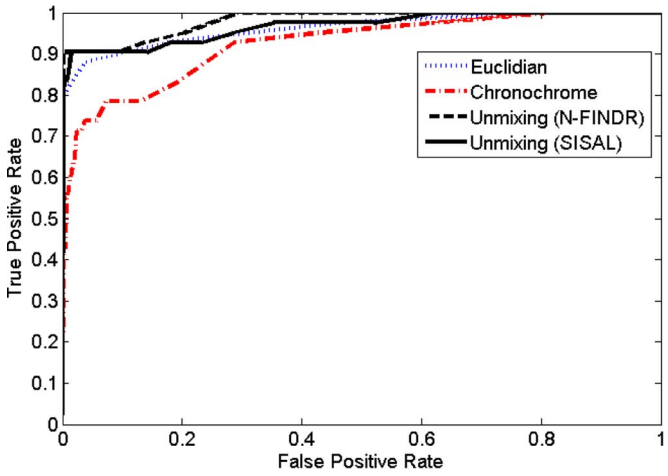

Fig. 8. ROC curves for the second synthetic data set.

Fig. 9. RGB images for the third synthetic data set.

provided, based on a manually prepared ground truth. Euclidian distance and the proposed change detection by unmixing approaches perform slightly better than CC, as in the previous case. However, note again that neither Euclidian distance nor CC provides the extra information shown in Fig. 6.

C. Synthetic Data Set 3

The third synthetic multitemporal data set is simulated from the well-known AVIRIS Salinas data set. The temporal data sets are of size 217 × 217 × 204 pixels. The spatial resolution of the data sets is 3.7 m. The RGB images of the temporal data sets are provided in Fig. 9. The synthetic change between the two temporal data sets is the region at the bottom of the image belonging to *Brocoli green weeds* class. Each pixel in this region is modified into one of the pixels in the *Celery* class region randomly. Ground truth data information for AVIRIS Salinas data is available from [19]. Additive Gaussian white noise is later added to each data set in 30-dB SNR.

The abundance maps for each temporal data set, obtained by FCLS after applying N-FINDR, are provided in Fig. 10. It can be observed, albeit with difficulty, that the fifth endmember becomes prominent, instead of the third, with respect to the first temporal data, for the pixels with change.

Fig. 11 gives a comparison between the final change maps obtained by EUC, CC, and the change detection by unmixing approach, using N-FINDR or SISAL as the EEA. It can be observed that EUC and CC give comparable results with that of the proposed approach. ROC curves, based on the ground truth change map, are provided in Fig. 12.

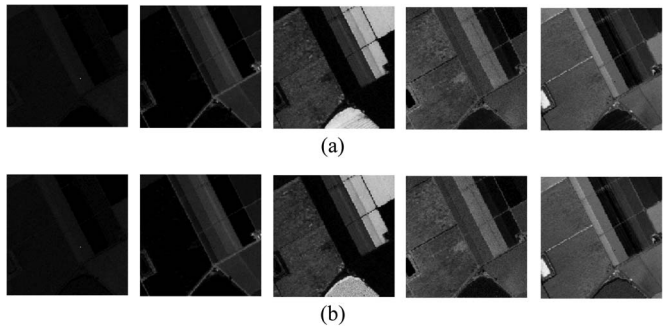

Fig. 10. Abundance maps. (a) For the first temporal data set. (b) For the second temporal data set.

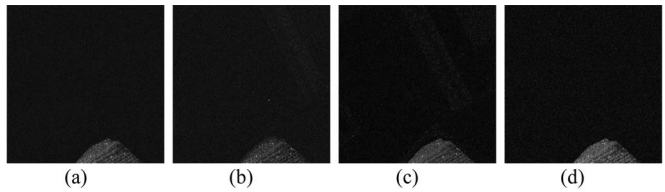

Fig. 11. Change maps for the third synthetic data set. (a) Euclidian distance. (b) CC. (c) Unmixing (N-FINDR as EEA). (d) Unmixing (SISAL as EEA).

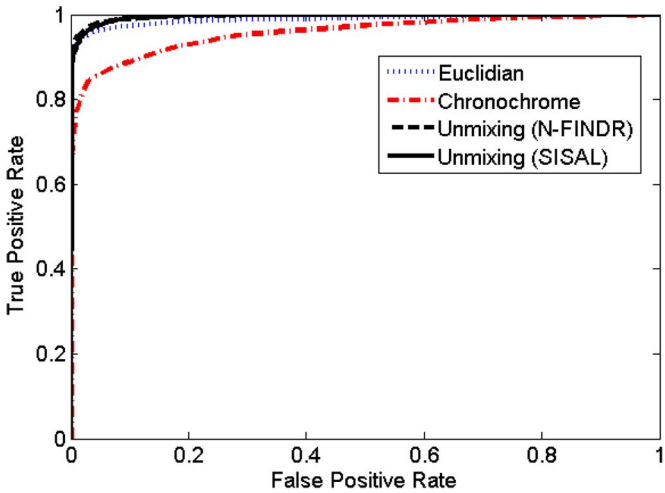

Fig. 12. ROC curves for the third synthetic data set.

IV. Experiments on Real Data

For the experiments on real data, subsets of two AVIRIS data sets have been used. The data sets are available in the AVIRIS database [20] and are from the Lower Michigan area from the dates: July 2009 and August 2011. The data sets have 224 spectral bands, and the spatial resolution of the data sets is around 16.7 m. The RGB images of the temporal data sets are provided in Fig. 13.

The final change maps obtained by unmixing and the change maps obtained by the other methods are provided in Fig. 14. Note that there are various changes in the scene between the two data acquisitions, including monthly changes in the crop signatures, illumination, and cloud coverage, which complicate the preparation of a ground truth map for change detection. In addition, the data sets have perspective variations between the two acquisitions, even though they are orthocorrected. Because of all these reasons, the obtained change maps are not very informative. However, the extra information that is available by

(a) (b)

Fig. 13. RGB images for the real data set. (a) 2009. (b) 2011.

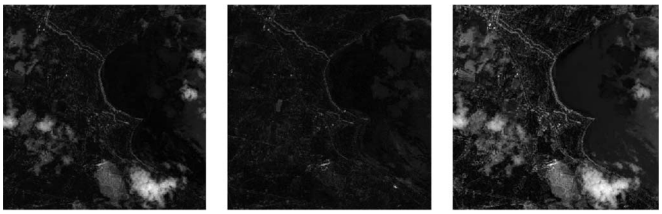

(a) (b) (c)

Fig. 14. Change maps for the third real data set. (a) Euclidian distance. (b) CC. (c) Unmixing.

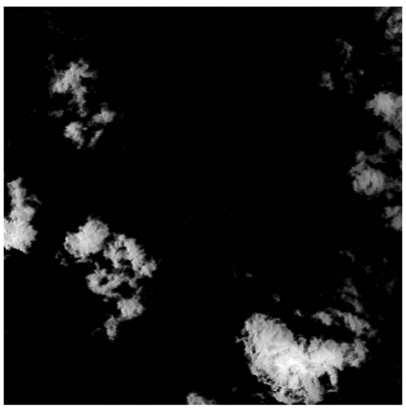

Fig. 15. Change map for the endmember corresponding to cloud spectra.

utilizing change detection by unmixing can be appreciated qualitatively in Fig. 15, which shows the abundance map difference between the two temporal data sets for one of the extracted endmembers. It is easy to deduce that this endmember corresponds to cloud spectra, and the cloud coverage difference between the two temporal data sets is observable through change detection by unmixing, unlike in other methods.

V. Conclusion and Future Research Lines

Although spectral unmixing is an important technique for analyzing remotely sensed hyperspectral data, hyperspectral change detection by unmixing has not been widely studied thus far. However, there are significant possibilities of this approach from the viewpoint of the information that can be obtained as the changes in the abundance maps provide information for each material in the scene discretely. This fact, combined with the flexibility and simple application of standard hyperspectral unmixing chains such as the one discussed in this letter, enables potential temporal summary of multitemporal data with many possible applications ranging from environmental monitoring to city planning. This letter has aimed to present the potential advantages of hyperspectral change detection by unmixing through various experimental results with both synthetic and real hyperspectral data.

Future studies may include the use of sparse unmixing based on spectral libraries for change detection purposes, the development of additional experimental results on real data sets, and taking the variability of endmember signatures with time into account.

References

[1] D. A. Landgrebe, *Signal Theory Methods in Multispectral Remote Sensing*. New York, NY, USA: Wiley, 2003.

[2] J. Meola, M. T. Eismann, R. L. Moses, and J. N. Ash, "Detecting changes in hyperspectral imagery using a model-based approach," *IEEE Trans. Geosci. Remote Sens.*, vol. 49, no. 7, pp. 2647–2661, Jul. 2011.

[3] A. Schaum and A. Stocker, "Long-interval chronochrome target detection," presented at the Int. Symp. Spectr. Sens. Res., San Diego, CA, USA, 1998.

[4] A. Schaum and A. Stocker, "Hyperspectral change detection and supervised matched filtering based on covariance equalization," in *Proc. SPIE*, 2004, vol. 5425, pp. 77–90.

[5] C. Wu, B. Du, and L. Zhang, "A subspace-based change detection method for hyperspectral images," *IEEE J. Sel. Topics Appl. Earth Observ. Remote Sens.*, vol. 6, no. 2, pp. 815–830, Apr. 2013.

[6] J. Theiler, C. Scovel, B. Wohlberg, and B. R. Roy, "Elliptically contoured distributions for anomalous change detection in hyperspectral imagery," *IEEE Geosci. Remote Sens. Lett.*, vol. 7, no. 2, pp. 271–275, Apr. 2010.

[7] A. A. Nielsen, "The regularized iteratively reweighted MAD method for change detection in multi- and hyperspectral data," *IEEE Trans. Image Process.*, vol. 16, no. 2, pp. 463–478, Feb. 2007.

[8] N. Keshava and J. F. Mustard, "Spectral unmixing," *IEEE Signal Process. Mag.*, vol. 19, no. 1, pp. 44–57, Jan. 2002.

[9] Q. Du, L. Wassom, and R. King, "Unsupervised linear unmixing for change detection in multitemporal airborne hyperspectral imagery," in *Proc. Int. Workshop Anal. Multi-Temporal Remote Sens. Images*, 2005, pp. 136–140.

[10] C.-C. Hsieh, P.-F. Hsieh, and C.-W. Lin, "Subpixel change detection based on abundance and slope features," in *Proc. IEEE IGARSS*, 2006, pp. 775–778.

[11] R. Zurita-Milla, L. Gomez-Chova, L. Guanter, J. G. P. W. Clevers, and G. Camps-Valls, "Multitemporal unmixing of medium-spatial-resolution satellite images: A case study using MERIS images for land-cover mapping," *IEEE Trans. Geosci. Remote Sens.*, vol. 49, no. 11, pp. 4308–4317, Nov. 2011.

[12] M. D. Iordache, J. M. Bioucas-Dias, and A. Plaza, "Sparse unmixing of hyperspectral data," *IEEE Trans. Geosci. Remote Sens.*, vol. 49, no. 6, pp. 2014–2039, Jun. 2011.

[13] J. M. Bioucas-Dias and J. M. P. Nascimento, "Hyperspectral subspace identification," *IEEE Trans. Geosci. Remote Sens.*, vol. 46, no. 8, pp. 2435–2445, Aug. 2008.

[14] M. E. Winter, "N-FINDR: An algorithm for fast autonomous spectral endmember determination in hyperspectral data," in *Proc. SPIE*, 1999, vol. 3753, pp. 266–277.

[15] J. M. P. Nascimento and J. M. Bioucas-Dias, "Vertex component analysis: A fast algorithm to unmix hyperspectral data," *IEEE Trans. Geosci. Remote Sens.*, vol. 43, no. 4, pp. 898–910, Apr. 2005.

[16] J. Li and J. Biucas-Dias, "Minimum volume simplex analysis: A fast algorithm to unmix hyperspectral data," in *Proc. IEEE IGARSS*, 2008, vol. 3, pp. 250–253.

[17] J. Bioucas-Dias, "A variable splitting augmented Lagragian approach to linear spectral unmixing," in *Proc. 1st IEEE WHISPERS*, 2009, pp. 1–4.

[18] D. Heinz and C. Chang, "Fully constrained least squares linear spectral mixture analysis method for material quantification in hyperspectral imagery," *IEEE Trans. Geosci. Remote Sens.*, vol. 39, no. 3, pp. 529–545, Mar. 2001.

[19] Computational Intelligence Group, Basque University, Spain, "Hyperspectral Remote Sensing Scenes." [Online]. Available: http://www.ehu.es/ccwintco/index.php?title=Hyperspectral_Remote_Sensing_Scenes&redirect=no

[20] Jet Propulsion Laboratory, NASA, "2006-2014 AVIRIS Flight Locator Tool." [Online]. Available: http://aviris.jpl.nasa.gov/alt_locator